Chemistry of Metals and Alloys

Chem. Met. Alloys 5 (2012) 103-112
Ivan Franko National University of Lviv
www.chemetal-journal.org

The {Y, Pr}–Ag–Si systems: isothermal sections and crystal structures

Igor SAVYSYUK[1*], Oleh SHCHERBAN[1], Nataliya SEMUSO[2], Roman GLADYSHEVSKII[2], Evgen GLADYSHEVSKII[2]

[1] *Scientific Consulting Company "Structure-Properties", Akad. Sakharova St. 33, 79026 Lviv, Ukraine*
[2] *Department of Inorganic Chemistry, Ivan Franko National University of Lviv, Kyryla i Mefodiya St. 6, 79005 Lviv, Ukraine*
* *Corresponding author. Tel.: +380-32-2402446; e-mail: sccstris@lviv.farlep.net*

Received May 28, 2012; accepted June 27, 2012; available on-line November 5, 2012

Isothermal sections of the phase diagrams were constructed at 1073 and 773 K for the Pr–Ag–Si system and at 873 K for the Y–Ag–Si system based on X-ray powder diffraction data. The crystal structures of two ternary compounds in the Pr–Ag–Si system were refined by the Rietveld method: $PrAg_2Si_2$, $CeAl_2Ga_2$-type structure, Pearson symbol *tI*10, space group *I*4/*mmm*, unit-cell parameters *a* = 0.42084(1), *c* = 1.06735(2) nm at 1073 K and $CeNi_{2+x}Sb_{2-x}$-type structure, *oI*10, *Immm*, *a* = 0.42088(2), *b* = 0.42287(2), *c* = 1.06695(3) nm at 773 K; PrAgSi, LiBaSi-type structure, *hP*3, *P*-6*m*2, *a* = 0.42302(1), *c* = 0.41911(1) nm at 1073 K and LaPtSi-type structure, *tI*12, $I4_1md$, *a* = 0.42087(2), *c* = 1.46432(8) nm at 773 K.

Rare-earth metal / Silver / Silicon / Phase diagram / Crystal structure / Solid solution

1. Introduction

The binary systems at the boundaries of the Y–Ag–Si and Pr–Ag–Si ternary systems have been studied and the phase diagrams have been constructed over the whole concentration region. Silver does not form binary compounds with silicon [1]. According to the phase diagrams [2,3], three and four binary compounds form in the Y–Ag and Pr–Ag systems: $Y_{14}Ag_{51}$, YAg_2, YAg, and $PrAg_5$, $Pr_{14}Ag_{51}$, $PrAg_2$, PrAg, respectively. Gokhale and Abbaschian [4] reported the formation of five binary yttrium silicides: YSi_2, Y_3Si_5, YSi, Y_5Si_4, and Y_5Si_3. In the work by Button *et al.* [5] the first compound was not observed and a new binary silicide, Y_2Si_3, was found in samples containing yttria as impurity phase. According to Eremenko *et al.* [6], five binary compounds form in the Pr–Si system: $PrSi_{2-x}$ with x = 0-0.2, Pr_3Si_4, PrSi, Pr_5Si_4, and Pr_5Si_3. Boutarek *et al.* [7] reported the existence of three defect disilicides $PrSi_{2-x}$ in the range of x = 0-0.4: two are orthorhombic (O_1 and O_2) and one is tetragonal (Q). Formation of Pr_3Si_2 is reported in [8]. Formation of Pr_2Si_{3-d}, d = 0.28 in samples annealed at 1373 K was observed by Schobinger-Papamantellos *et al.* [9]. Crystallographic data of the binary compounds in the {Y, Pr}–{Ag, Si} systems are summarized in Table 1.

Three ternary compounds were previously known in the {Y, Pr}–Ag–Si systems: YAgSi (ZrNiAl-type structure, Pearson symbol *hP*9, space group *P*-62*m*) [11], $PrAg_2Si_2$ ($CeAl_2Ga_2$, *tI*10, *I*4/*mmm*) [12], and $PrAg_{0.67}Si_{1.33}$ ($Pr_3Ag_2Si_4$) (AlB_2, *hP*3, *P*6/*mmm*) [11]. Our preliminary results on the $PrAg_2$–$PrSi_2$ section were reported in [13].

The aim of the present work was to determine the phase equilibria in the {Y, Pr}–Ag–Si systems and the crystal structures of the compounds in these and related systems.

2. Experimental

The samples were prepared from high-purity components (rare-earth metals > 99.9 wt.%, silver > 99.98 wt.%, and silicon > 99.99 wt.%) by arc melting under an argon atmosphere on a water-cooled copper crucible. To ensure homogeneity, the buttons were turned and re-melted. The weight loss of the initial total mass was lower than 1 wt.%. Then the as-cast buttons were annealed for one month at 873 K in the case of Y-, Tb- and Ho-containing alloys. For the Pr–Ag–Si system, the alloys were annealed for two months at 773 K, or for three weeks at 1073 K. All the samples were annealed in evacuated silica tubes and then quenched in water.

Table 1 Crystallographic parameters of the binary compounds (literature data).

Compound	Structure type	Pearson symbol	Space group	Unit-cell parameters, nm			Ref.
				a	*b*	*c*	
$Y_{14}Ag_{51}$	$Gd_{14}Ag_{51}$	*hP*68	*P*6/*m*	1.2637	–	0.9300	[10]
YAg_2	$MoSi_2$	*tI*6	*I*4/*mmm*	0.3691	–	0.9241	[10]
YAg	CsCl	*cP*2	*Pm*-3*m*	0.3619	–	–	[10]
$PrAg_5$	$CaCu_5$	*hP*6	*P*6/*mmm*	...	...	...	[3]
$Pr_{14}Ag_{51}$	$Gd_{14}Ag_{51}$	*hP*68	*P*6/*m*	1.2846	–	0.9746	[10]
α-$PrAg_2$	KHg_2	*oI*12	*Imma*	0.4781	0.7084	0.8196	[10]
α-$PrAg_2$	AlB_2	*hP*3	*P*6/*mmm*	0.4777	–	0.6867	[10]
PrAg	CsCl	*cP*2	*Pm*-3*m*	0.3739	–	–	[10]
α-YSi_2	α-$GdSi_2$	*oI*12	*Imma*	0.404	0.395	1.323	[10]
β-YSi_2	α-$ThSi_2$	*tI*12	$I4_1/amd$	0.404	–	1.342	[10]
$YSi_{1.56}$	AlB_2	*hP*3	*P*6/*mmm*	0.3843	–	0.4143	[10]
YSi	CrB	*oS*8	*Cmcm*	0.4251	1.0526	0.3826	[10]
Y_5Si_4	Sm_5Ge_4	*oP*36	*Pnma*	0.7390	1.452	0.7640	[10]
Y_5Si_3	Mn_5Si_3	*hP*16	$P6_3/mcm$	0.8418	–	0.6337	[10]
$PrSi_{2-x}$ (Q), x=0	α-$ThSi_2$	*tI*12	$I4_1/amd$	0.4200	–	1.3733	[7]
$PrSi_{2-x}$ (O_2), x=0.2	α-$GdSi_2$	*oI*12	*Imma*	0.4159	0.4149	1.3716	[7]
$PrSi_{2-x}$ (O_1), x=0.4	α-$GdSi_2$	*oI*12	*Imma*	0.4166	0.4112	1.3819	[7]
Pr_2Si_{3-d}, d=0.28	V_2B_3	*oS*20	*Cmcm*	0.43834	2.47200	0.39326	[9]
PrSi	FeB	*oP*8	*Pnma*	0.829	0.394	0.594	[10]
Pr_5Si_4	Zr_5Si_4	*tP*36	$P4_12_12$	0.790	–	1.491	[10]
Pr_3Si_2	U_3Si_2	*tP*10	*P*4/*mbm*	0.775	–	0.438	[8]
Pr_5Si_3	Cr_5B_3	*tI*32	*I*4/*mcm*	0.7812	–	1.3772	[10]

Table 2 Crystallographic parameters of the binary silicides (this work, system Y–Si at 873 K, system Pr–Si at 1073 K).

Compound	Structure type	Pearson symbol	Space group	Unit-cell parameters, nm		
				a	*b*	*c*
YSi_2	α-$GdSi_2$	*oI*12	*Imma*	0.4056(1)	0.3963(2)	1.3437(4)
$YSi_{1.67}$	AlB_2	*hP*3	*P*6/*mmm*	0.3840(1)	–	0.4150(2)
YSi	CrB	*oS*8	*Cmcm*	0.4261(1)	1.0534(2)	0.3832(1)
Y_5Si_4	Sm_5Ge_4	*oP*36	*Pnma*	0.7399(4)	1.4578(5)	0.7693(5)
Y_5Si_3	Mn_5Si_3	*hP*16	$P6_3/mcm$	0.84174(9)	–	0.63165(8)
$PrSi_{2-1.70}$ (Q)	α-$ThSi_2$	*tI*12	$I4_1/amd$	0.4201(1)-0.4163(1)	–	1.3744(3)-1.3754(4)
$PrSi_{1.63}$ (O)	α-$GdSi_2$	*oI*12	*Imma*	0.4162(1)	0.4103(1)	1.3827(3)
PrSi	FeB	*oP*8	*Pnma*	0.8244(2)	0.3943(1)	0.5928(2)
Pr_5Si_4	Zr_5Si_4	*tP*36	$P4_12_12$	0.7925(3)	–	1.4962(7)
Pr_3Si_2	U_3Si_2	*tP*10	*P*4/*mbm*	0.7772(4)	–	0.4337(3)
Pr_5Si_3	Cr_5B_3	*tI*32	*I*4/*mcm*	0.7827(3)	–	1.379(1)

The isothermal section of the phase diagram of the Y–Ag–Si system was constructed based on the study of 82 alloys; 106 samples were prepared for the Pr–Ag–Si system. Preliminary phase analysis was carried out based on diffraction patterns obtained with Debye-Scherrer cameras (diameter 53.7 mm), using Cr *K* radiation. The unit-cell parameters were refined on X-ray diffraction data from polycrystalline samples, recorded on a diffractometer DRON-2.0 (Fe *K*α radiation). The programs PowderCell [14] and LATCON [15] were used for the calculations. The observed diffraction intensities were compared with reference powder patterns of known binary and ternary phases.

The crystal structure determinations were based on X-ray diffraction data from polycrystalline samples, recorded on diffractometers DRON-4.07 (Cu *K*α radiation) and Philips PW1820 (Cu *K*α radiation). Rietveld refinements were performed using the DBWS-9407 program [16].

Table 3 Crystallographic parameters of ternary compounds in *R*–Ag–Si systems (873 K).

Compound	Structure type	Pearson symbol	Space group	Unit-cell parameters, nm		
				a	*b*	*c*
YAg_2Si_2	$CeAl_2Ga_2$	*tI*10	*I*4/*mmm*	0.41214(6)	–	1.0749(2)
$YAg_{1.4\text{-}1.0}Si_{0.6\text{-}1.0}$	Fe_2P/ZrNiAl	*hP*9	*P*-62*m*	0.7137(1)-0.70181(5)	–	0.4152(1)-0.41662(6)
YAgSi [11]	ZrNiAl	*hP*9	*P*-62*m*	0.7024	–	0.4170
$YAg_{0.7}Si_{1.3}$	AlB_2	*hP*3	*P*6/*mmm*	0.41220(7)	–	0.4019(1)
$YAg_{0.6}Si_{1.4}$	α-$ThSi_2$	*tI*12	$I4_1/amd$	0.40688(9)	–	1.4233(5)
$YAg_{0.4\text{-}0.2}Si_{1.6\text{-}1.8}$	α-$ThSi_2$	*tI*12	$I4_1/amd$	0.40535(9)-0.40320(7)	–	1.3801(7)-1.3780(5)
$PrAg_2Si_2$[a]	$CeAl_2Ga_2$	*tI*10	*I*4/*mmm*	0.42084(1)	–	1.06735(2)
$PrAg_2Si_2$ [12]	$CeAl_2Ga_2$	*tI*10	*I*4/*mmm*	0.4235	–	1.068
$PrAg_2Si_2$[b]	$CeNi_{2+x}Sb_{2-x}$	*oI*10	*Immm*	0.42088(2)	0.42287(2)	1.06695(3)
$PrAg_{1.2\text{-}0.7}Si_{0.8\text{-}1.3}$[a]	AlB_2	*hP*3	*P*6/*mmm*	0.4260(2)-0.4255(3)	–	0.4152(2)-0.4159(4)
$PrAg_{0.67}Si_{1.33}$ [11]	AlB_2	*hP*3	*P*6/*mmm*	0.4253	–	0.4157
$PrAg_{1.2\text{-}1.1}Si_{0.8\text{-}0.9}$[b]	AlB_2	*hP*3	*P*6/*mmm*	0.4249(3)	–	0.4123(2)
PrAgSi[a]	LiBaSi	*hP*3	*P*-6*m*2	0.42302(1)	–	0.41911(1)
PrAgSi[b]	LaPtSi	*tI*12	$I4_1md$	0.42087(2)	–	1.46432(8)
$TbAg_2Si_2$	$CeAl_2Ga_2$	*tI*10	*I*4/*mmm*	0.4134(1)	–	1.0724(3)
TbAgSi	ZrNiAl	*hP*9	*P*-62*m*	0.7047(1)	–	0.4191(1)
$TbAg_{0.7}Si_{1.3}$	AlB_2	*hP*3	*P*6/*mmm*	0.4133(2)	–	0.4036(5)
$TbAg_{0.3}Si_{1.7}$	α-$ThSi_2$	*tI*12	$I4_1/amd$	0.4056(1)	–	1.3821(7)
HoAgSi	ZrNiAl	*hP*9	*P*-62*m*	0.6996(1)	–	0.4159(2)

[a] at 1073 K; [b] at 773 K.

3. Results and discussion

Five binary compounds with silver, $Y_{14}Ag_{51}$, YAg_2, YAg, $Pr_{14}Ag_{51}$, and PrAg were observed in the binary alloys. The existence of $PrAg_2$ was confirmed in our previous work [17], but was not observed in the ternary alloys with silicon. Crystallographic data for the rare-earth metal silicides as determined in this work are given in Table 2. Eleven binary silicides: YSi_2, $YSi_{1.67}$, YSi, Y_5Si_4, Y_5Si_3, $PrSi_{2-x}$ (Q), $PrSi_{2-x}$ (O), PrSi, Pr_5Si_4, Pr_3Si_2, and Pr_5Si_3, were observed at the temperatures of investigation. The unit-cell parameters and composition of the orthorhombic non-stoichiometric disilicide $PrSi_{2-x}$ (O) (x = 0.37) are close to the data reported in [7] for the phase $PrSi_{2-x}$ (O_1). The second orthorhombic disilicide reported in [7] was not observed, but the tetragonal disilicide $PrSi_{2-x}$ (Q) has a homogeneity range (x = 0-0.30) that covers the ranges of the phases Q and O_2. The unit-cell parameters and homogeneity ranges of the non-stoichiometric disilicides $PrSi_{2-x}$ (Q) and (O) are shown in Fig. 1.

The isothermal section of the phase diagram of the Y–Ag–Si system at 873 K is shown in Fig. 2. No significant solubility of the third component in the binary compounds was observed. Formation of five ternary compounds was found (Table 3). The unit-cell volume of the $YAg_{1.4\text{-}1.0}Si_{0.6\text{-}1.0}$ compound with Fe_2P/ZrNiAl-type structure

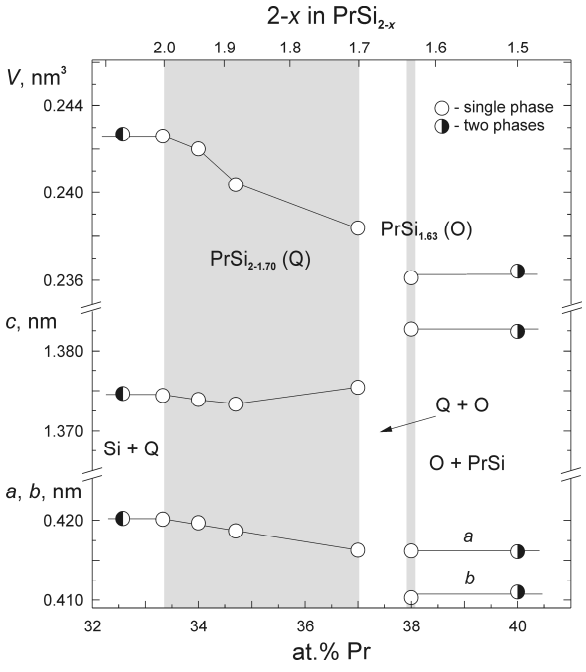

Fig. 1 Unit-cell parameters and homogeneity ranges of the non-stoichiometric praseodymium disilicides Q and O.

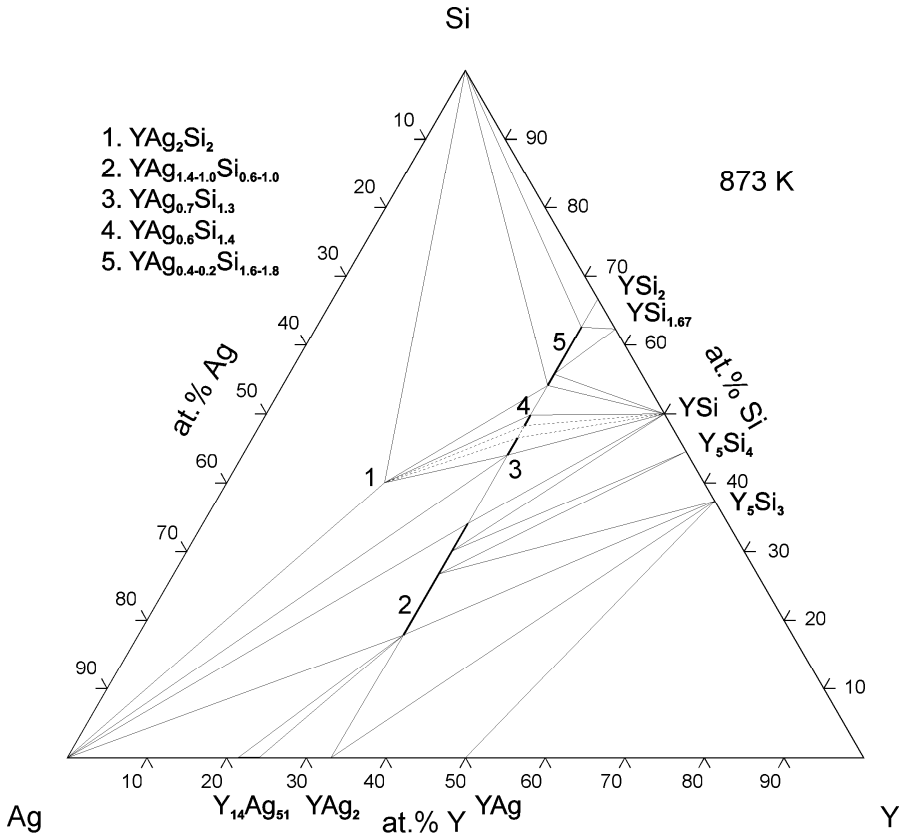

Fig. 2 Isothermal section of the Y–Ag–Si phase diagram at 873 K.

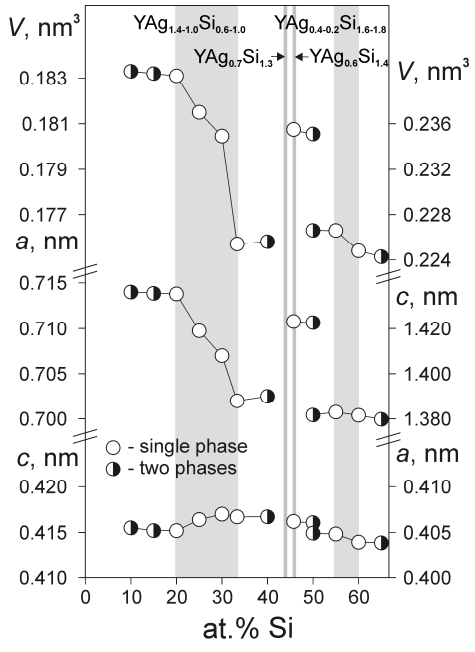

Fig. 3 Unit-cell parameters and homogeneity ranges of the ternary compounds at the isoconcentrate of 33.3 at.% Y.

decreases almost linearly with increasing Si content from 20 to 30 at.% and drops at the equiatomic composition (Fig. 3). The other four compounds in the system Y–Ag–Si are: YAg_2Si_2 ($CeAl_2Ga_2$-type structure), $YAg_{0.7}Si_{1.3}$ (AlB_2), $YAg_{0.6}Si_{1.4}$ and $YAg_{0.4\text{-}0.2}Si_{1.6\text{-}1.8}$ (both α-$ThSi_2$). Isostructural compounds were found in systems with Tb and Ho (see Table 3).

The isothermal section of the phase diagram of the Pr–Ag–Si system at 1073 K is shown in Fig. 4. A broad solid solution based on $PrSi_{2-x}$ (Q) forms in the system (Fig. 5). The solubility of silver extends to 18.6 at.% at 33.3 at.% Pr and reaches a maximum of 21.7 at.% at 35.5 at.% Pr. The unit-cell parameter *c* increases almost linearly on replacing Si by Ag (Fig. 6), while the parameter *a* remains approximately constant. The solid solubility of silver in the other binaries is relatively low: less than 3 at.% for PrSi (a = 0.8264(3), b = 0.3954(2), c = 0.5926(3) nm), < 3 at.% for Pr_5Si_4 (a = 0.7930(3), c = 1.4967(4) nm), about 5 at.% for Pr_3Si_2 (a = 0.7786(4), c = 0.4339(2) nm, Fig. 7), and < 4 at.% for Pr_5Si_3 (a = 0.7820(3), c = 1.383(1) nm).

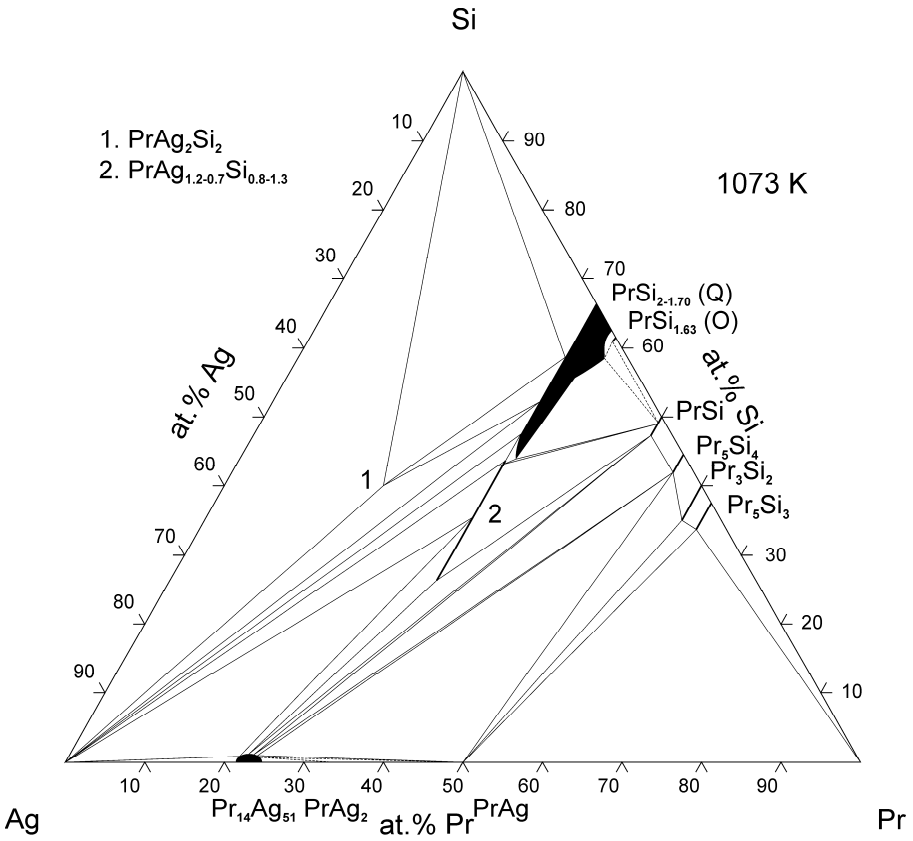

Fig. 4 Isothermal section of the Pr–Ag–Si phase diagram at 1073 K.

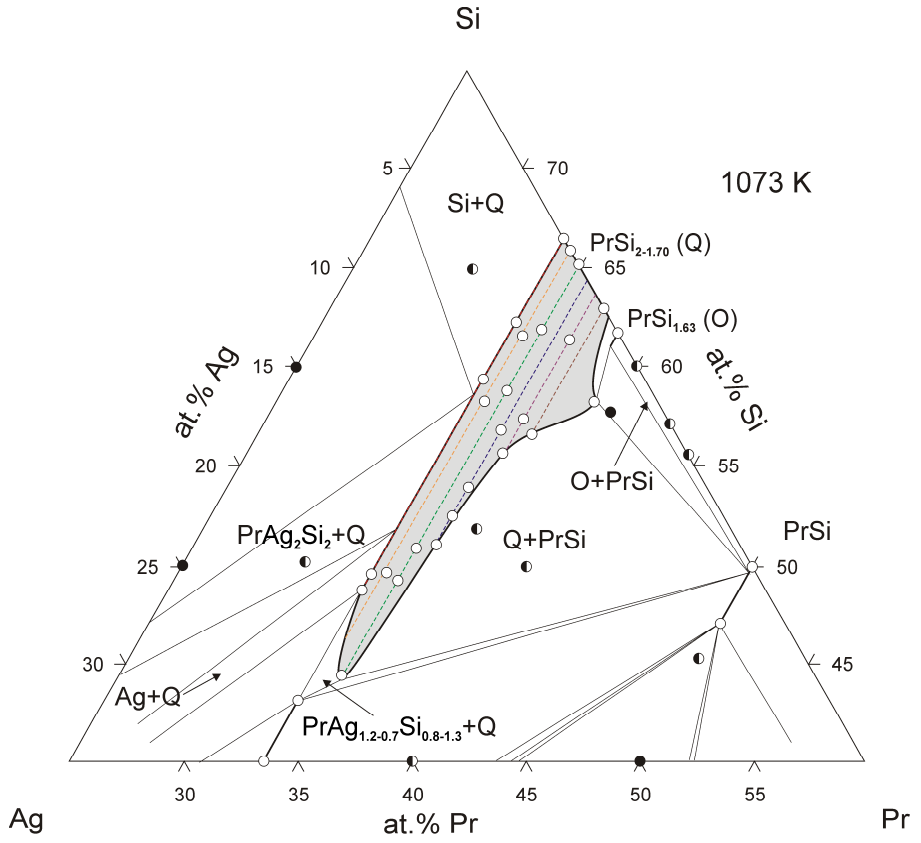

Fig. 5 Homogeneity range of the solid solution of silver in the praseodymium disilicide Q at 1073 K. Isoconcentrates of Pr are drawn in color as a guide for the eyes.

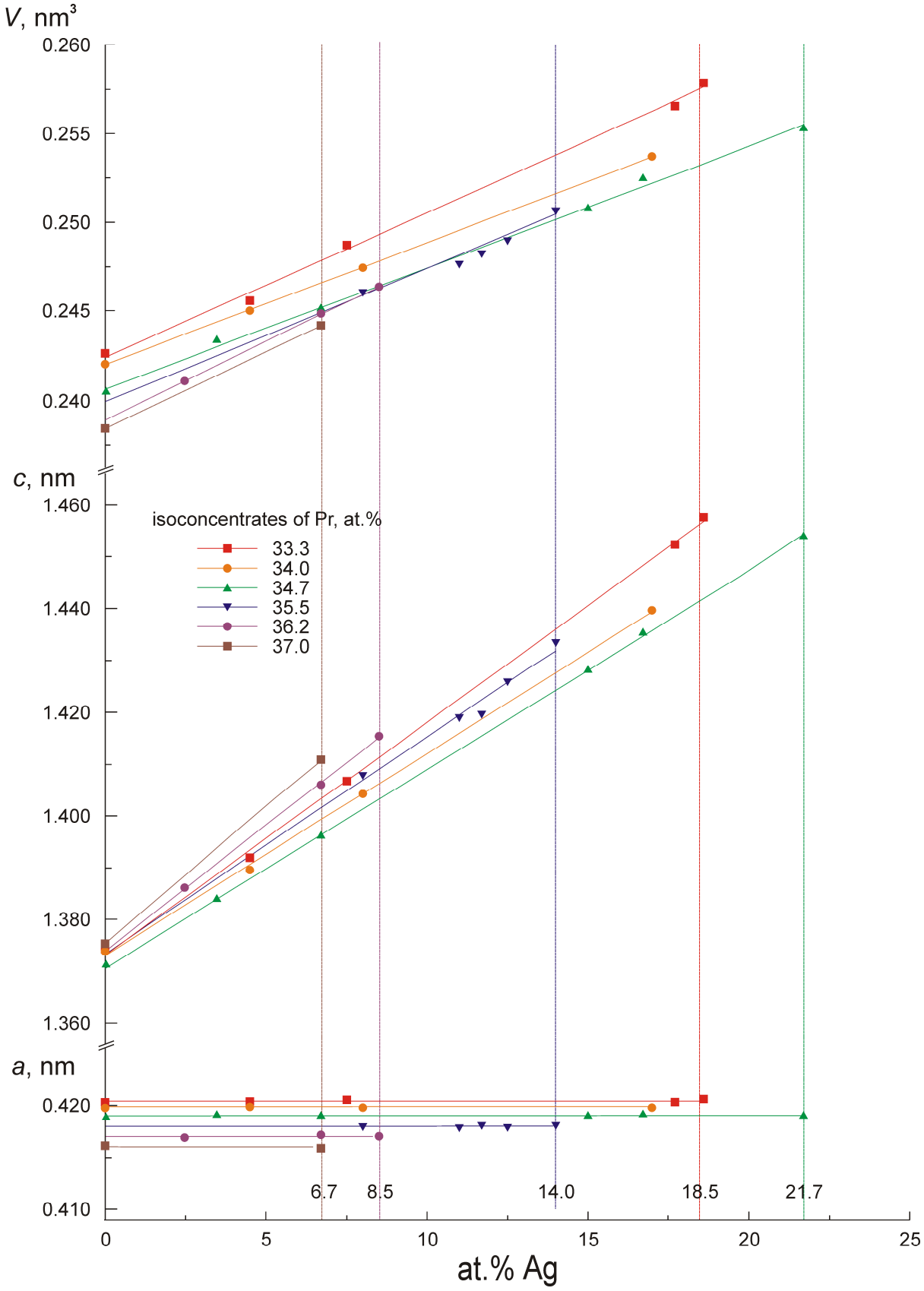

Fig. 6 Unit-cell parameters of the solid solution of silver in the praseodymium disilicide Q at 1073 K. The isoconcentrates of Pr correspond to Fig. 5.

Two ternary compounds form in the Pr–Ag–Si system at 1073 K (Tables 3 and 4, Figs. 8 and 9). $PrAg_2Si_2$ has a tetragonal $CeAl_2Ga_2$-type structure with unit-cell parameters close to those reported by Mayer *et al.* [12]. A refinement carried out on a sample annealed at 773 K shows distortion of the unit cell to an orthorhombic $CeNi_{2+x}Sb_{2-x}$-type structure. The compound with AlB_2-type structure, $PrAg_{1.2\text{-}0.7}Si_{0.8\text{-}1.3}$, has a significant homogeneity range of 26.5-42.0 at.% Si. The unit-cell parameters at the Si-poor and Si-rich boundaries are similar (Fig. 10), but the unit-cell volume drops significantly near the equiatomic composition. The Rietveld refinement indicates LiBaSi-type of ordering for the composition PrAgSi. At 773 K the homogeneity range of the AlB_2-type phase is smaller, $PrAg_{1.2\text{-}1.1}Si_{0.8\text{-}0.9}$ (Fig. 11), and no trend towards ordering of Ag and Si atoms was observed. At high silicon content the LaPtSi-type ordered phase PrAgSi is in equilibrium with the solid solution of Ag in $PrSi_{2-x}$ (Q). The plot of the unit-cell volume for the α-$ThSi_2$-type solution at 33.3 at.% Pr shows that for the ordered phase the volume is significantly smaller than the extrapolated value (Fig. 12). No changes of the homogeneity ranges of the solutions of Ag in the binary phases of the Pr–Si system were observed with respect to the isothermal section at 1073 K.

4. Conclusions

Isothermal sections of the phase diagram were constructed at 1073 and 773 K for the Pr–Ag–Si system. Two ternary compounds exist at 1073 K:

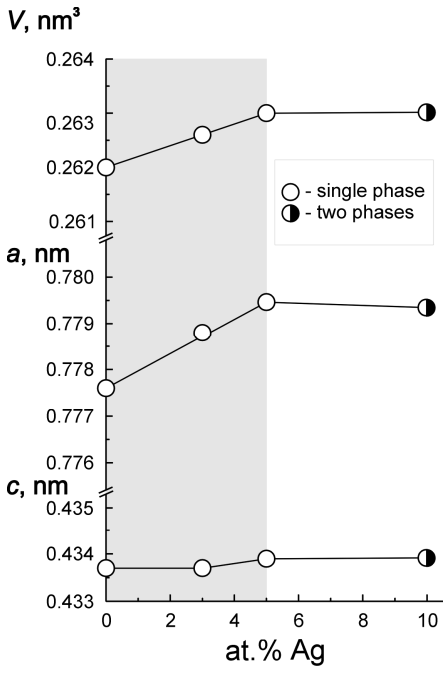

Fig. 7 Unit-cell parameters and homogeneity range of the solid solution of silver in Pr_3Si_2.

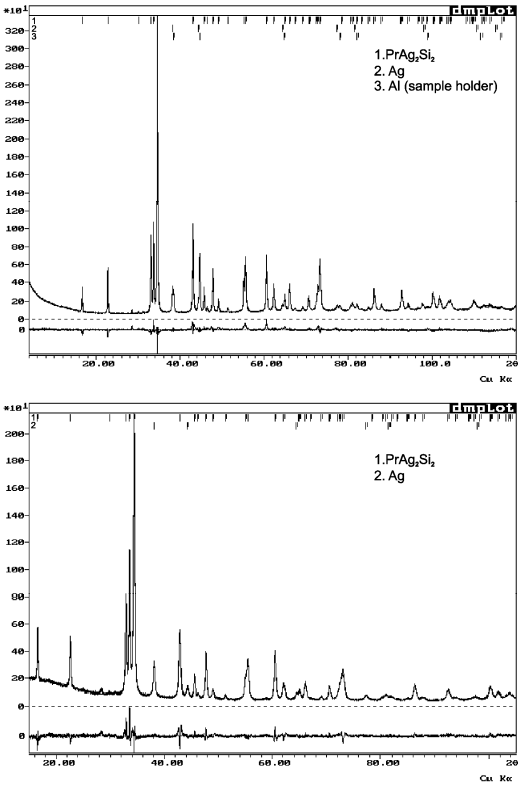

Fig. 8 Rietveld refinement on X-ray diffraction patterns recorded for a $Pr_{20}Ag_{40}Si_{40}$ alloy annealed at 1073 K (top) and 773 K (bottom).

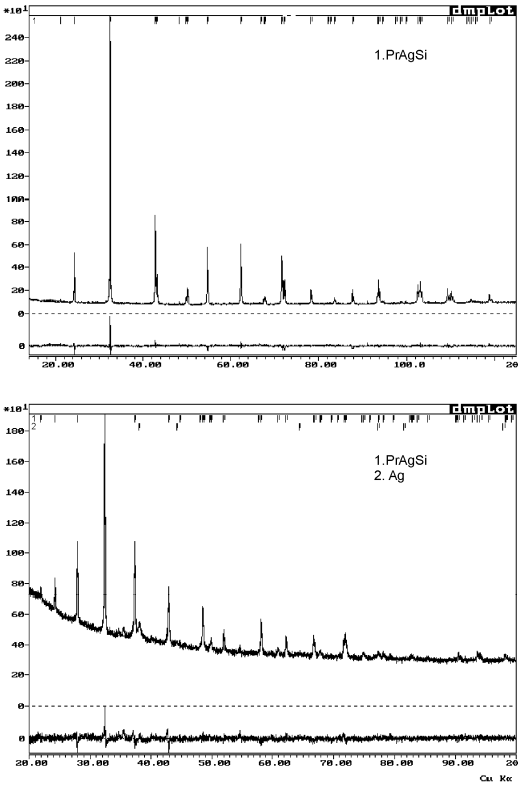

Fig. 9 Rietveld refinement on X-ray diffraction patterns recorded for a $Pr_{33.3}Ag_{33.3}Si_{33.4}$ alloy annealed at 1073 K (top) and 773 K (bottom).

Table 4 Results of the Rietveld refinements for ternary compounds in the Pr–Ag–Si system: atomic coordinates and isotropic displacement parameters.

Site	Wyckoff position	*x*	*y*	*z*	B_{iso}, 10^{-2} nm^2
$PrAg_2Si_2$ (1073 K), $CeAl_2Ga_2$, *tI*10, *I*4/*mmm*,					
a = 0.42084(1), *c* = 1.06735(2) nm,					
Philips PW1820 (Cu *K*α), R_p = 0.0519, R_{wp} = 0.0691					
Pr	2*a*	0	0	0	0.15(4)
Ag	4*d*	0	½	¼	0.63(1)
Si	4*e*	0	0	0.3949(3)	0.51(2)
$PrAg_2Si_2$ (773 K) $CeNi_{2+x}Sb_{2-x}$, *oI*10, *Immm*,					
a = 0.42088(2), *b* = 0.42287(2), *c* = 1.06695(3) nm,					
DRON-4.07 (Cu *K*α), R_p = 0.0553, R_{wp} = 0.0721					
Pr	2*a*	0	0	0	1.98(4)
Ag	4*j*	½	0	0.2495(5)	1.92(3)
Si	4*i*	0	0	0.3951(4)	3.6(1)
PrAgSi (1073 K), LiBaSi, *hP*3, *P*-6*m*2,					
a = 0.42302(1), *c* = 0.41911(1) nm,					
DRON-4.07 (Cu *K*α), R_p = 0.0443, R_{wp} = 0.0569					
Pr	1*d*	⅔	⅓	½	0.73(4)
Ag	1*e*	⅓	⅔	0	0.64(7)
Si	1*a*	0	0	0	0.5(2)
PrAgSi (773 K), LaPtSi, *tI*12, $I4_1md$,					
a = 0.42087(2), *c* = 1.46432(8) nm,					
DRON-4.07 (Cu *K*α), R_p = 0.0251, R_{wp} = 0.0322					
Pr	4*a*	0	0	0.5832(3)	0.6(3)
Ag	4*a*	0	0	0.1658(5)	0.9(4)
Si	4*a*	0	0	0.0000(4)	0.8(6)

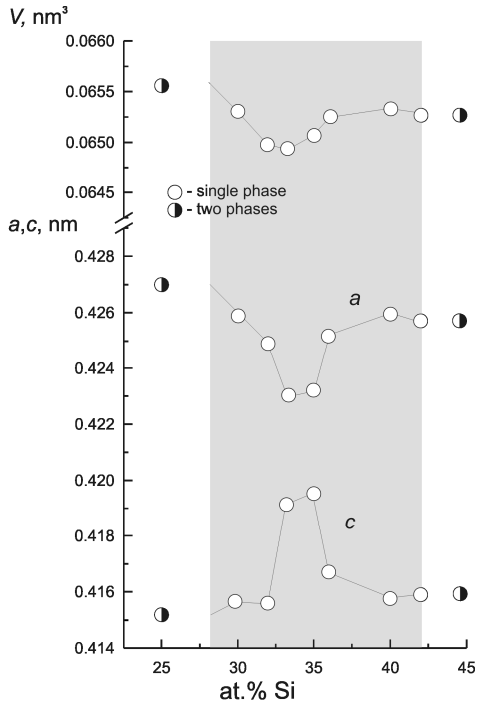

Fig. 10 Unit-cell parameters and homogeneity range of $PrAg_{1.2\text{-}0.7}Si_{0.8\text{-}1.3}$.

$PrAg_2Si_2$ with $CeAl_2Ga_2$-type structure and $PrAg_{1.2\text{-}0.7}Si_{0.8\text{-}1.3}$ with AlB_2-type structure (LiBaSi-type ordering at the equiatomic composition). At 773 K the $PrAg_2Si_2$ compound is characterized by distortion of the unit cell and its structure corresponds to the orthorhombic $CeNi_{2+x}Sb_{2-x}$ type. The homogeneity range of the AlB_2-type compound is smaller at 773 K and does not include the equiatomic composition, $PrAg_{1.2\text{-}1.1}Si_{0.8\text{-}0.9}$. At this temperature PrAgSi adopts a tetragonal LaPtSi-type structure. Similarly to the systems with La and Ce, a broad solid solution of silver in the disilicide $PrSi_{2-x}$ (Q) with α-$ThSi_2$-type structure forms in the Pr–Ag–Si system.

The isothermal section of the phase diagram of the Y–Ag–Si system was studied at 873 K. It is characterized by the existence of five ternary compounds: YAg_2Si_2, $YAg_{1.4\text{-}1.0}Si_{0.6\text{-}1.0}$, $YAg_{0.7}Si_{1.3}$, $YAg_{0.6}Si_{1.4}$, and $YAg_{0.4\text{-}0.2}Si_{1.6\text{-}1.8}$. The structures of YAg_2Si_2 and $YAg_{0.7}Si_{1.3}$ belong to the $CeAl_2Ga_2$ and AlB_2 types, respectively, like the structures of $PrAg_2Si_2$ and $PrAg_{1.2\text{-}0.7}Si_{0.8\text{-}1.3}$ at 1073 K. An Fe_2P-type structure is observed for $YAg_{1.4\text{-}1.0}Si_{0.6\text{-}1.0}$ (ZrNiAl-type ordering at the equiatomic composition). Two other compounds in the Y–Ag–Si system adopt α-$ThSi_2$-type structures, however, with different *c*/*a* ratios.

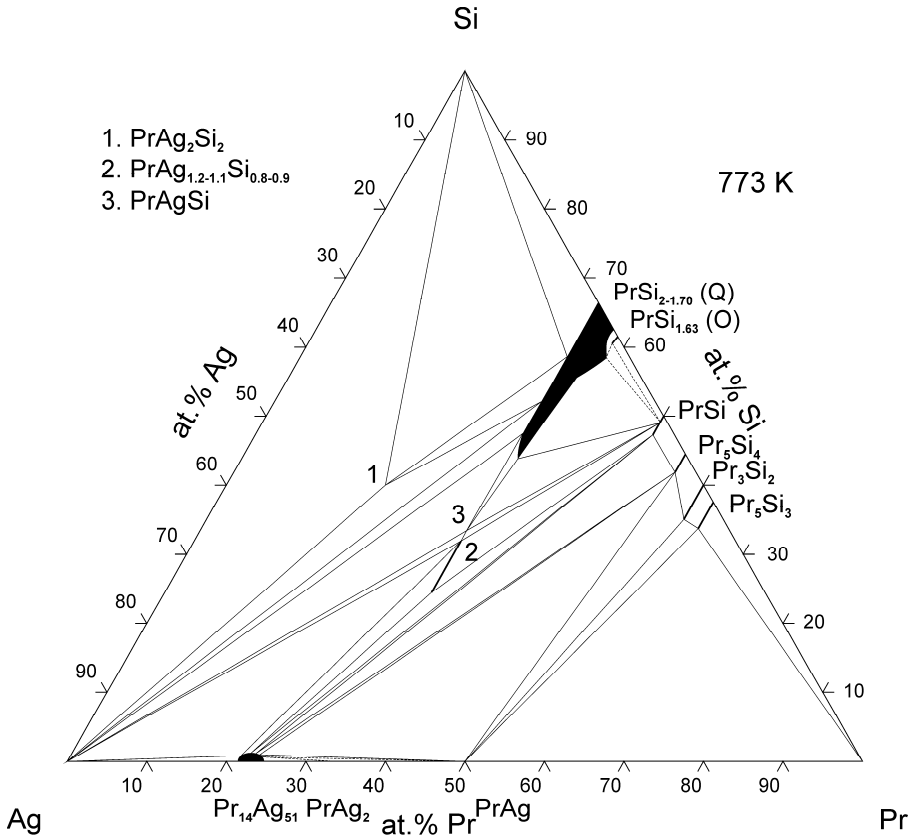

Fig. 11 Isothermal section of the Pr–Ag–Si phase diagram at 773 K.

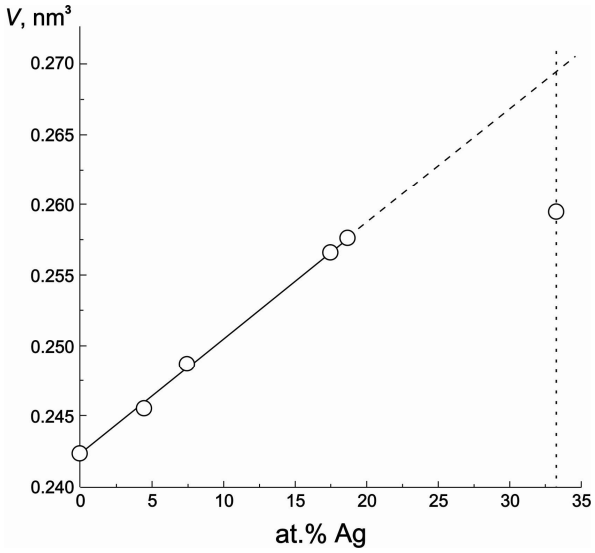

Fig. 12 Unit-cell volume of the α-$ThSi_2$-type solid solution $PrAg_xSi_{2-x}$ (x = 0-0.56) and LaPtSi-type ordered phase PrAgSi at 773 K.

References

[1] R.W. Olesinski, A.B. Gokhale, G.J. Abbaschian, *Bull. Alloy Phase Diagrams* 10 (1989) 635-640.

[2] K.A. Gschneidner, Jr., F.W. Calderwood, *Bull. Alloy Phase Diagrams* 4 (1983) 57-62.

[3] K.A. Gschneidner, Jr., F.W. Calderwood, *Bull. Alloy Phase Diagrams* 6 (1985) 23-26.

[4] A.B. Gokhale, G.J. Abbaschian, *Bull. Alloy Phase Diagrams* 7 (1986) 485-489.

[5] T.W. Button, I.J. McColm, J.M. Ward, *J. Less-Common Met.* 159 (1990) 205-222.

[6] V.N. Eremenko, K.A. Meleshevich, Yu.I. Buyanow, *Izv. Vyssh. Uchebn. Zaved., Tsvetn. Metall.* 3 (1986) 82-87.

[7] N. Boutarek, J. Pierre, B. Lambert-Andron, Ph. L'Heritier, R. Madar, *J. Alloys Compd.* 204 (1994) 251-260.

[8] E.I. Gladyshevskii, *Izv. Akad. Nauk SSSR, Neorg. Mater.* 1 (1965) 706-710.

[9] P. Schobinger-Papamantellos, K.H.J. Buschow, P. Fischer, *J. Magn. Magn. Mater.* 114 (1992) 131-137.

[10] P. Villars, K. Cenzual (Eds.), *Pearson's Crystal Data. Crystal Structure Database for Inorganic Compounds*, Release 2012/13, ASM International, Materials Park (OH).

[11] A. Iandelli, *J. Less-Common Met.* 113 (1985) L25-L27.

[12] I. Mayer, J. Cohen, I. Felner, *J. Less-Common Met.* 30 (1973) 181-184.

[13] M.M. Dzioba, I.A. Savysyuk, O.O. Shcherban, E.I. Gladyshevskii, *Visn. Lviv. Univ., Ser. Khim.* 36 (1996) 59-65.
[14] W. Kraus, G. Nolze, *PowderCell for Windows*, Version 2.4, Federal Institute for Materials Research and Testing, Berlin, 2000.
[15] D. Schwarzenbach, *LATCON: Refine Lattice Parameters*, University of Lausanne, Lausanne, 1966.
[16] R.A. Young, A. Sakthivel, T.S. Moss, C.O. Paiva-Santos, *J. Appl. Crystallogr.* 28 (1995) 366-367.
[17] I.A. Savysyuk, R.E. Gladyshevskii, E.I. Gladyshevskii, *J. Alloys Compd.* 314 (2001) 167-169.